Model-based Predictive control of a concentrated solar plant for heat production

Eliott Girard[1] and Stéphane Thil[1] and Julien Eynard[1] and Stéphane Grieu[1]

***Abstract*— Industrial heat processes are one of the most energy-intensive and polluting activities in the industry. Concentrated solar energy could be used to supply thermal energy to industrial processes, however, the intermittency of this energy source makes it difficult to satisfy a specific energy demand. Adaptation to this high variability can be achieved by using real-time control of solar plants in combination with energy storage systems. To address this issue, this paper presents a real-time control strategy of a parabolic trough solar plant used to produce industrial heat. The control strategy uses a Model-based Predictive Control (MPC) method based on an optimization algorithm, with the objective of satisfying a heat demand by modifying the mass flow rate of the heat transfer fluid in the storage system, which is a thermocline tank. In order to determine the behaviour of the solar plant, the optimization algorithm requires forecasts of solar irradiance, however, it is well-known that short-term forecasts of this quantity are difficult to obtain due to atmospheric disturbances. Therefore, the influence of forecast errors has been assessed to ensure the robustness of the control strategy using available forecast models: a smart persistence of incident solar energy and a model relying on the analysis of ground-based sky images. The integration of these predictions has also been studied to reduce the performance loss due to forecast errors by adapting the forecast horizon and integrating measured data.**

I. INTRODUCTION

Decarbonization of the industrial sector is a major challenge to reduce climate change. Thermal energy is one of the most consumed energy types by industrial processes and is mainly provided by natural gas combustion. Concentrated Solar Thermal (CST) seems a relevant carbon-free alternative for industrial heat production, due to its high conversion efficiency [1]. Furthermore, this technology can provide thermal energy on a wide temperature range [2], [3]. An industrial heat process is characterized by both the required temperature and the thermal power demand; therefore, CST plants need to adapt to the high variability of solar irradiance to meet these requirements. In order to limit these variations, CST plants usually include energy storage systems [3], which have to be controlled to satisfy the thermal power demand.

In Section II, we present a control strategy to satisfy a heat demand applied to a small-scale CST plant. This plant is equipped with three parabolic trough solar collectors, for a recoverable thermal power of 150 kW. It is equipped with a thermocline tank to store energy and heat exchangers for transferring thermal power to an industrial process. A heat transfer fluid flows between these three systems. The plant works between a low fluid temperature of 220 °C and a high fluid temperature of 300 °C [4]. The thermocline tank stores both hot and cold fluid with a temperature gradient along the height of the tank. This temperature level is adequate for various industrial processes such as food processing, textile treatment or paper production [1]. The simplified architecture of this power plant is given in Figure 1, while Table I details the most important variables.

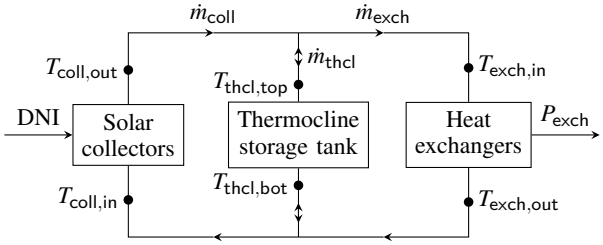

Fig. 1: Interactions between the three systems.

TABLE I: Variables describing the CST plant.

	Description	Unit
$\dot{m}_{coll}$	Mass flow inside the solar collectors	$kg\,s^{-1}$
$\dot{m}_{thcl}$	Upward mass flow inside the thermocline tank	$kg\,s^{-1}$
$\dot{m}_{exch}$	Mass flow inside the heat exchangers	$kg\,s^{-1}$
P_{exch}	Transferred power through the heat exchangers	W
P_{demand}	Thermal power demand	W
DNI	Direct Normal Irradiance	$W\,m^{-2}$
$T_{coll,in}$	HTF temperature at the inlet of the solar collectors	°C
$T_{coll,out}$	HTF temperature at the outlet of the solar collectors	°C
$T_{thcl,bot}$	HTF temperature at the bottom of the thermocline tank	°C
$T_{thcl,top}$	HTF temperature at the top of the thermocline tank	°C
$T_{exch,in}$	HTF temperature at the inlet of the heat exchangers	°C
$T_{exch,out}$	HTF temperature at the outlet of the heat exchangers	°C
A_{coll}	Surface covered by the solar collectors	m^2
V_{coll}	Volume inside the solar collectors absorber tube	m^3
η_{coll}	Efficiency of the solar collectors	–
ρ_f	Density of the heat transfer fluid	$kg\,m^{-3}$
c_f	Heat capacity of the heat transfer fluid	$J\,K^{-1}\,kg^{-1}$

A common issue in CST plant operation is that solar irradiance is hard to forecast, due to the complex behaviour

[1]PROMES-CNRS laboratory (UPR-8521), University of Perpignan Via Domitia, France

of clouds. Many methods involving physical modelling, machine learning or deep learning have already been developed [5], but some models based on the analysis of ground-based sky images seem promising for short-term forecasting [6], [7], [8]. As we must ensure our control strategy can adapt to DNI forecast errors, a robustness analysis is presented in Section III. An improvement of the DNI forecast integration is then presented in Section IV to reduce the performance loss due to these forecast errors.

Literature on control of solar plants mainly focuses on control strategy development [9], [10], and little on robustness to perturbations such as DNI prediction error [11], [12]. Furthermore, only few studies integrate a thermocline storage tank in a control strategy [13], [14].

II. CONTROL STRATEGY DESCRIPTION

The control strategy relies on adapting the storage tank operation to DNI variations. Its objective is to satisfy the required heat demand by modifying the upward fluid mass flow inside the thermocline tank $\dot{m}_{\mathsf{thcl}}$. The implemented control strategy is based on Model-based Predictive Control (MPC), since this is a widely used strategy in the concentrated solar context [15], [16], [17]. The MPC strategy consists in finding the best control inputs over a sliding horizon, applying only the first control input to the CST plant and repeating these steps by shifting the sliding horizon. This control strategy is relevant in situations in which we need to take into account the future system states to determine the current control inputs, which is often the case in the CST context due to DNI variability. In our case, the best control inputs are determined using an optimization algorithm that minimizes the deviation between the power transferred to the industrial process P_{exch} and the heat demand P_{demand}, while satisfying mass flow constraints (a negative $\dot{m}_{\mathsf{thcl}}$ means the thermocline tank is charging). The optimization problem solved at each iteration, using Sequential Quadratic Programming (SQP), is formulated in Equation (1).

$$\begin{aligned} \min_{\dot{m}_{\mathsf{thcl}} \in \mathbb{R}^n} \quad & \sqrt{\sum_{i=0}^{n-1} \left(P_{\mathsf{exch}}(k+i) - P_{\mathsf{demand}}(k+i)\right)^2} \\ \text{s.t.} \quad & 0 < \dot{m}_{\mathsf{thcl}}(k+i) + \dot{m}_{\mathsf{coll}}(k+i) < \dot{m}_{\mathsf{max}}, \\ & \forall i \in [\![0, n-1]\!] \end{aligned} \tag{1}$$

In this equation, the index k represents the starting time step of the current optimization horizon. The exchanged power P_{exch} needs to be determined as a function of $\dot{m}_{\mathsf{thcl}}$, which is achieved by modelling the temperature of the heat transfer fluid that circulates in the CST plant [18]. This modelling relies on thermodynamic interactions occurring inside the thermocline tank and the solar collectors to determine the heat exchangers inlet fluid temperature $T_{\mathsf{exch,in}}$, thus calculating the exchanged power using Equation (2), with a fixed outlet fluid temperature $T_{\mathsf{exch,out}} = 220\,^{\circ}\mathrm{C}$:

$$P_{\mathsf{exch}} = (\dot{m}_{\mathsf{coll}} + \dot{m}_{\mathsf{thcl}}) c_{\mathsf{f}} (T_{\mathsf{exch,in}} - T_{\mathsf{exch,out}}) \tag{2}$$

Furthermore, the mass flow inside the solar collectors $\dot{m}_{\mathsf{coll}}$ is determined before the optimization starts so that the collectors outlet fluid temperature value is stabilized around the high temperature of $T_{\mathsf{coll,out}} = 300\,^{\circ}\mathrm{C}$, using the forecasted DNI values. The mass flow is calculated from the inlet fluid temperature $T_{\mathsf{coll,in}}$, the collectors efficiency η_{coll}, the solar field surface A_{coll} and the fluid properties, using Equation (3):

$$\begin{aligned} \rho_{\mathsf{f}} V_{\mathsf{coll}} c_{\mathsf{f}} \frac{\mathrm{d}T_{\mathsf{coll,out}}}{\mathrm{d}t} = \mathrm{DNI} \eta_{\mathsf{coll}} A_{\mathsf{coll}} \\ - \dot{m}_{\mathsf{coll}} c_{\mathsf{f}} (T_{\mathsf{coll,out}} - T_{\mathsf{coll,in}}) \end{aligned} \tag{3}$$

This thermodynamic equation assumes that the fluid temperature inside the solar collectors is homogeneous. Despite simplifying the real system, it stills provides satisfying inputs to maintain the required temperature [18].

An estimation of the optimal mass flow in the thermocline tank $\dot{m}_{\mathsf{thcl}}$ is computed to initialize the optimization algorithm. If the solar collectors can gather enough power to satisfy the heat demand, the thermocline tank is charged with the excess production and $\dot{m}_{\mathsf{thcl}}$ is determined using Equation (4). In the other case, the storage tank is discharged to provide the missing thermal power to meet the heat demand and $\dot{m}_{\mathsf{thcl}}$ is determined using Equation (5).

$$\dot{m}_{\mathsf{thcl}} = \begin{cases} \dfrac{P_{\mathsf{demand}}}{c_f (T_{\mathsf{coll,out}} - T_{\mathsf{exch,out}})} - \dot{m}_{\mathsf{coll}}, \\ \qquad \text{if } \dot{m}_{\mathsf{coll}} c_f (T_{\mathsf{coll,out}} - T_{\mathsf{exch,out}}) \geqslant P_{\mathsf{demand}} \end{cases} \tag{4}$$

$$\dot{m}_{\mathsf{thcl}} = \begin{cases} \dfrac{P_{\mathsf{demand}} - \dot{m}_{\mathsf{coll}} c_f (T_{\mathsf{coll,out}} - T_{\mathsf{exch,out}})}{c_f (T_{\mathsf{thcl,top}} - T_{\mathsf{exch,out}})}, \\ \qquad \text{if } \dot{m}_{\mathsf{coll}} c_f (T_{\mathsf{coll,out}} - T_{\mathsf{exch,out}}) < P_{\mathsf{demand}} \end{cases} \tag{5}$$

Each MPC iteration is separated by $\Delta t = 30\,\mathrm{s}$ and the optimization horizon is $n\Delta t = 120\,\mathrm{s}$, these hyperparameters were proven to give satisfying results regarding deviation from the objective, maximum demand overshoot and optimization execution time [18]. The optimized mass flow for the current time step $\dot{m}^*_{\mathsf{thcl}}(k)$ is then applied to an accurate model of the thermocline tank [19] and the solar collectors [20] in order to simulate the plant's response to this control input.

An example of control results is presented in Figure 2. The DNI values used for this simulation, presented in Figure 2a, were measured the on October, 11, 2019, starting at 9 a.m.; for this example only, we assume that the DNI values are perfectly forecasted. The mass flow inside the solar collectors $\dot{m}_{\mathsf{coll}}$ and the optimized mass flow inside the thermocline tank $\dot{m}^*_{\mathsf{thcl}}$ are plotted in Figure 2b; we can note that the thermocline tank alternates between charge ($\dot{m}_{\mathsf{thcl}} < 0$) and discharge ($\dot{m}_{\mathsf{thcl}} > 0$) to account for the solar collectors cutting off during drops of DNI. The resulting exchanged power P_{exch} and the heat demand, which is constant at 30 kW, are presented in Figure 2c. The exchanged power meets the heat demand with small deviations and overshoots despite the highly varying DNI of an overcast sky situation. Finally, Figure 2d zooms in on the heat demand to better highlight exchanged power fluctuations. Since we are using perfect forecasts, the observed deviations only come from modelling errors in the objective function.

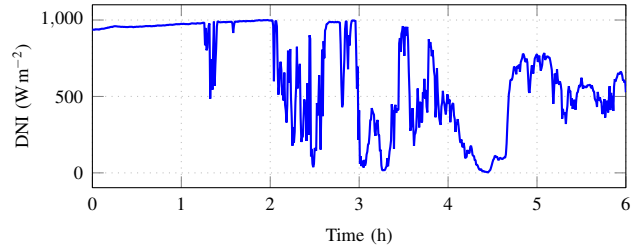

(a) Measured DNI values.

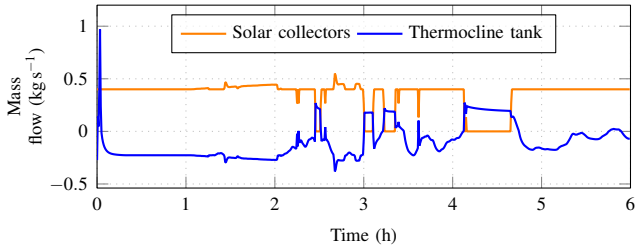

(b) Mass flow inside the solar collectors and the thermocline tank.

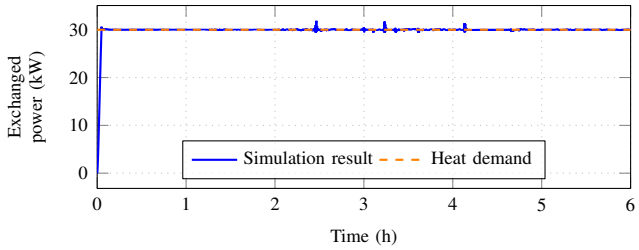

(c) Thermal power transferred through the heat exchangers.

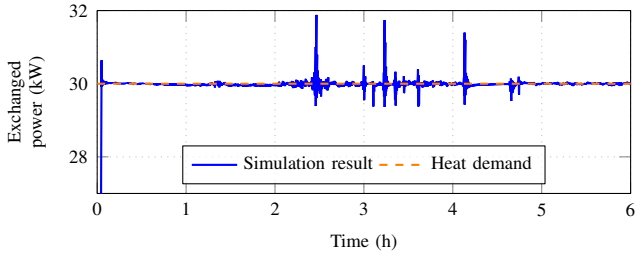

(d) Thermal power transferred through the heat exchangers (zoomed around the heat demand).

Fig. 2: Results of the control strategy in the case of perfect forecast.

III. INFLUENCE OF DNI FORECAST ERRORS

In order to assess the robustness of this control strategy, we can assess the control performance degradation when using actual DNI forecasts, taking into consideration two criteria: the deviation from the heat demand and the maximum overshoot. Two forecast models have been used: the smart persistence and an advanced image-based model [8].

The smart persistence model assumes that the DNI absorption from atmospheric disturbances is constant over the forecast horizon. The DNI can be expressed as Equation (6):

$$\mathrm{DNI} = k_c \mathrm{DNI}_{\mathrm{cs}} \tag{6}$$

where:

- $\mathrm{DNI}_{\mathrm{cs}}$ is the DNI value that would be measured if the sky was clear of atmospheric disturbances; it can be determined using an available model [21];
- k_c is the clear-sky index, depicting the percentage of DNI absorbed by atmospheric disturbances; this is the value that is considered constant over the forecast horizon when using the smart persistence model.

The image-based forecast model (called hybrid model) is more complex: it relies both on past DNI measurements and ground-based sky images to forecast solar irradiance. The sky images are analysed to determine the cloud motion and several neural networks are applied to the input data to determine image and DNI features and finally the DNI forecast. Since this forecast method is complex, the reader is referred to the original article for its full description [8].

Figure 3 shows the forecasted DNI values for a forecast horizon of 15 min according to the two models along with measured values. The hybrid model produces more accurate forecasts than the smart persistence model, and is able to detect DNI ramps more precisely. Indeed, the Root Mean Square Error (RMSE) between measured and forecasted DNI values is 6.49 W m^{-2} when using the smart persistence model and 4.47 W m^{-2} when using the hybrid model. The measured DNI is the one used in Figure 2 to simulate the perfect forecast.

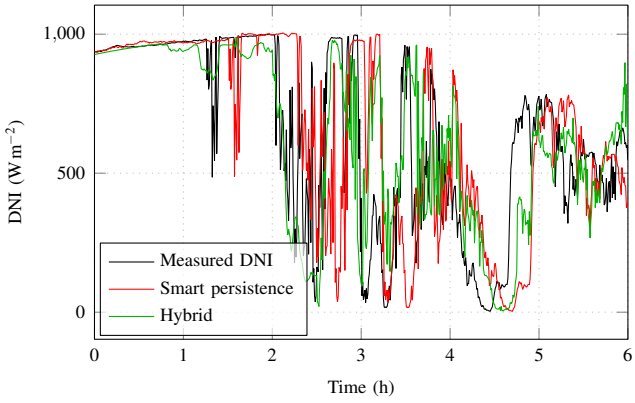

Fig. 3: 15 min-ahead forecasts of DNI according to the two forecast methods.

To analyze the robustness of our control algorithm, we can compare the performance drop of the control algorithm by using the DNI forecasts provided by the smart persistence or the hybrid model (with a 15 min forecast horizon), as presented in Table II. We can see that we only get slight deviations from the objective and little to no increase in the overshoot for both forecast methods. The hybrid model performs best and even accidentally reduces the maximum overshoot. In can also be noticed that despite the lack of precision of the smart persistence model on this long forecast horizon, the control algorithm still manages to maintain a low deviation from the objective. Figure 4 presents results when using the hybrid model: the mass flows (Figure 4b) are similar to those obtained with perfect forecast, while the

exchanged power fluctuations (Figure 4d) are more important in this situation.

TABLE II: Performance of the control strategy using DNI forecasts.

	Deviation from the objective (kWh)	Maximum overshoot (%)
Perfect forecast	0.991	6.27
Smart persistence model	2.10	8.62
Hybrid model	1.82	6.10

The integration of forecasted DNI values could be improved to reduce the performance drop of the control algorithm. Indeed, the chosen forecast horizon of 15 min is not adapted to the optimization horizon of 120 s. Since forecasts on shorter horizons are usually more accurate [7], [8], the control strategy could benefit from adapting the forecast horizon to the optimization horizon. Additionally, we can update the past DNI forecasts at every MPC iteration to improve their accuracy using the shortest forecast horizon possible. This requires the hybrid model to be executed many times during the control process, which can be done since its execution time is rather low, at around 1.6 s [8].

IV. IMPROVING DNI FORECASTS INTEGRATION

As discussed in Section III, the integration of DNI forecasts can be improved. The control algorithm uses DNI values to determine the mass flow inside the solar collectors $\dot{m}_{\text{coll}}$ using Equation (3) over the optimization horizon of 120 s. Therefore, at the time t, we only need DNI values in the interval $[t,\ t+120\,\text{s}[$.

We can then provide the control algorithm with measured DNI for the first time step and forecasted DNI for the remaining time steps. Since we are using a 30 s-long time step, we only require DNI forecasts at t+30 s, t+60 s and t+90 s. This improved DNI forecast integration method was also used in similar works [22]. On these very short-term horizons, the forecast models presented in Section III give more accurate DNI values. DNI data measured on March 1, 2022 starting at 8 a.m., typical of a clear-sky situation with some cloudy events, are presented in Figure 5, along with forecasted DNI values over a horizon of 90 s. The RMSE between measured and forecasted data is 0.74 W m^{-2} using the smart persistence model and 0.14 W m^{-2} using the hybrid model. Both the smart persistence and hybrid model perform well with this forecast horizon.

The results obtained with perfect forecast are presented in Figure 6. The exchanged power quickly matches the heat demand as in the previous situation; however, the small instabilities are lower due to less varying DNI values, as shown in Figure 6c. We can also notice in Figure 6a that the mass flow inside the solar collectors reaches a maximum value: this is due to the thermocline storage tank being full of hot fluid, therefore increasing the solar collectors inlet temperature. In this case, the collectors are slightly defocused to avoid overheating the heat transfer fluid by curtailing the incident solar energy. This situation creates small deviations in the exchanged power.

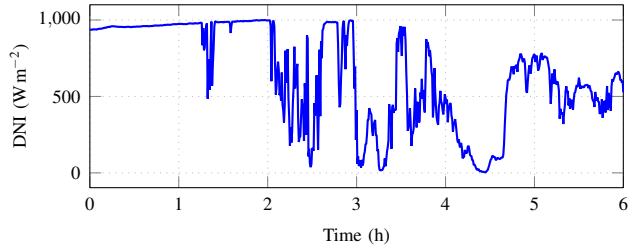

(a) Measured DNI values.

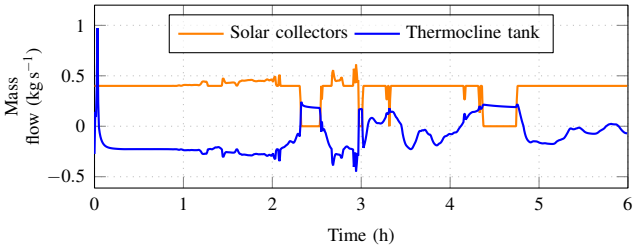

(b) Mass flow inside the solar collectors and the thermocline tank.

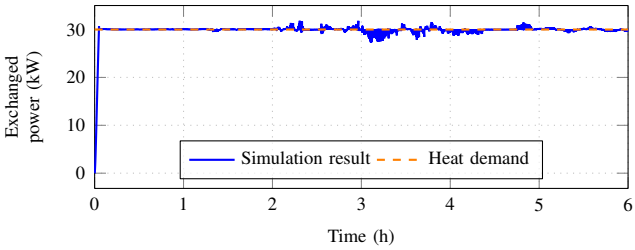

(c) Thermal power transferred through the heat exchangers.

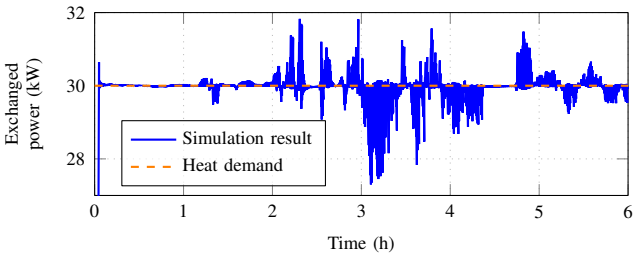

(d) Thermal power transferred through the heat exchangers (zoomed around the heat demand).

Fig. 4: Results of the control strategy with hybrid forecast model.

The results obtained using actual DNI forecasts are presented in Table III. The loss in the deviation from the objective and the maximum overshoot are almost nonexistent for both forecast models. For understanding purposes, the relative increase in the deviation from the objective, compared to the results obtained with perfect forecast, is equal to 0.008 % for the smart persistence model and 0.003 % for the hybrid model. This is due to better forecast accuracy and the integration of measured DNI values to correct forecast

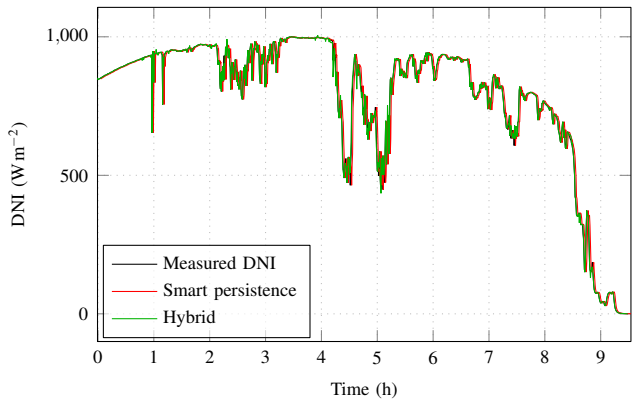

Fig. 5: 90 s-ahead forecasts of DNI values with the smart persistence and hybrid models.

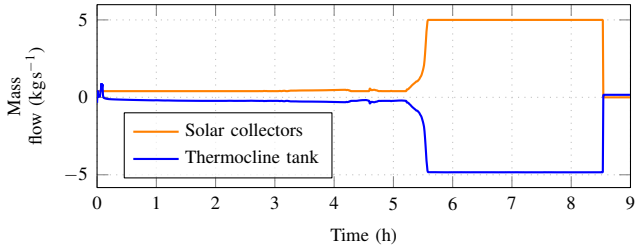

(a) Mass flow inside the solar collectors and the thermocline tank.

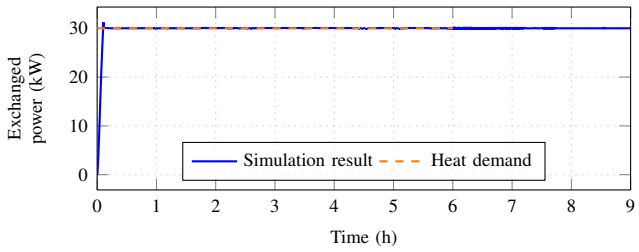

(b) Thermal power transferred through the heat exchangers.

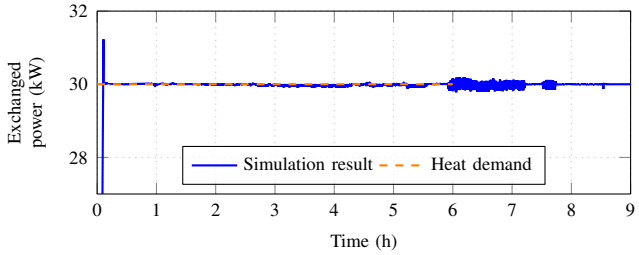

(c) Thermal power transferred through the heat exchangers (zoomed around the heat demand).

Fig. 6: Results of the control strategy with perfect forecast for the adapted forecast horizon situation.

errors. As a comparison, the results obtained using the hybrid forecast model are presented in Figure 7. There is almost no difference with perfect forecast, instabilities only come from the inherent modelling errors. These results show the robustness to forecast errors of the control strategy in this situation, and we can expect it to behave in the same way on varied DNI data.

TABLE III: Performance of the control strategy with improved DNI forecast integration.

	Deviation from the objective (kWh)	Maximum overshoot (%)
Perfect forecast	1.79	4.10
Smart persistence model	1.79	4.10
Hybrid model	1.79	4.10

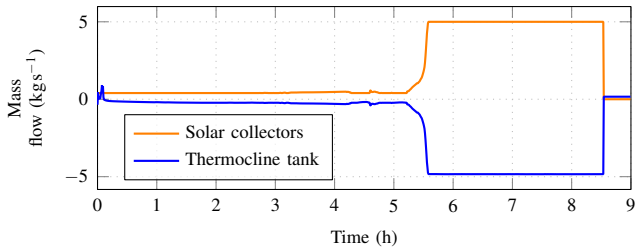

(a) Mass flow inside the solar collectors and the thermocline tank.

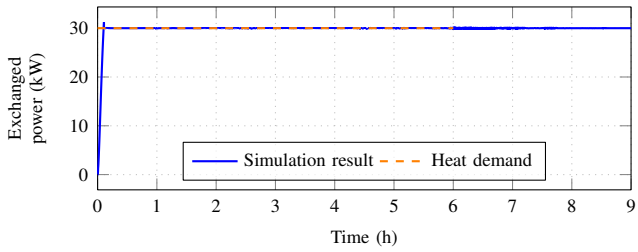

(b) Thermal power transferred through the heat exchangers.

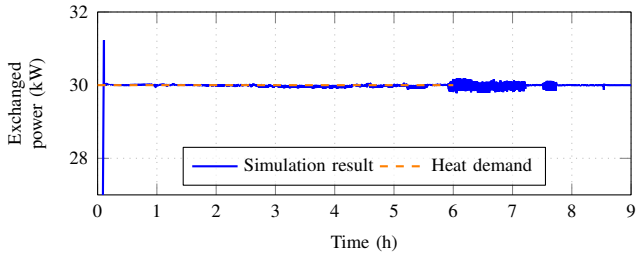

(c) Thermal power transferred through the heat exchangers (zoomed around the heat demand).

Fig. 7: Results of the control strategy with improved DNI forecast integration using the hybrid model.

V. CONCLUSION

This paper presents a control strategy intended for concentrated solar thermal plants aiming at satisfying an industrial process heat demand. The strategy relies on the Model-based

Predictive Control (MPC); an optimization algorithm is used to find the best control inputs. An analysis of the robustness of the strategy has been conducted to ensure it performs well in case of forecast errors. The analysis is based on two criteria: the deviation from the objective and the maximum overshoot. An improvement of DNI forecast integration into the control algorithm has then been implemented to reduce the performance drop due to forecast errors. The obtained results show that the control strategy is still reliable with almost no loss in deviation from the objective and maximum overshoot.

In order to ensure the reliability of this control strategy on varied situations, we also need to evaluate it according to different thermal power demands. Finally, implementation on a real CST plant and experimental validation of the control strategy are necessary to prove its relevance.

ACKNOWLEDGMENT

This work was supported by the French Investments for the future ("Investissements d'Avenir") program managed by the French National Research Agency (ANR) under contract ANR-10-LABX-22-01 (Labex SOLSTICE). This work benefited from State aid managed by the National Research Agency (ANR) under the program France 2030 with the reference "ANR-22-PESP-0005" (SHIP4D).

REFERENCES

[1] A. K. Sharma et al. "Solar Industrial Process Heating: A Review". In: *Renewable and Sustainable Energy Reviews* 78 (Oct. 1, 2017), pp. 124–137. ISSN: 1364-0321. DOI: 10.1016/j.rser.2017.04.079.

[2] K. Ravi Kumar, N. V. V. Krishna Chaitanya, and N. Sendhil Kumar. "Solar Thermal Energy Technologies and Its Applications for Process Heating and Power Generation – A Review". In: *Journal of Cleaner Production* 282 (Feb. 1, 2021), p. 125296. ISSN: 0959-6526. DOI: 10.1016/j.jclepro.2020.125296.

[3] S. Kalogirou. "The Potential of Solar Industrial Process Heat Applications". In: *Applied Energy* 76.4 (Dec. 1, 2003), pp. 337–361. ISSN: 0306-2619. DOI: 10.1016/S0306-2619(02)00176-9.

[4] N. Boullet et al. "MicroSol-R: Versatile Solar Facility for Research and Industry". In: *AIP Conference Proceedings* 2033.1 (Nov. 8, 2018), p. 030003. ISSN: 0094-243X. DOI: 10.1063/1.5067019.

[5] A. Gupta, K. Gupta, and S. Saroha. "A Review and Evaluation of Solar Forecasting Technologies". In: *Materials Today: Proceedings*. International Conference on Materials and System Engineering 47 (Jan. 1, 2021), pp. 2420–2425. ISSN: 2214-7853. DOI: 10.1016/j.matpr.2021.04.491.

[6] Y. Chu et al. "Real-Time Forecasting of Solar Irradiance Ramps with Smart Image Processing". In: *Solar Energy* 114 (Apr. 1, 2015), pp. 91–104. ISSN: 0038-092X. DOI: 10.1016/j.solener.2015.01.024.

[7] M. Caldas and R. Alonso-Suárez. "Very Short-Term Solar Irradiance Forecast Using All-Sky Imaging and Real-Time Irradiance Measurements". In: *Renewable Energy* 143 (Dec. 1, 2019), pp. 1643–1658. ISSN: 0960-1481. DOI: 10.1016/j.renene.2019.05.069.

[8] Y. Karout et al. "Hybrid Intrahour DNI Forecast Model Based on DNI Measurements and Sky-Imaging Data". In: *Solar Energy* 249 (Jan. 1, 2023), pp. 541–558. ISSN: 0038-092X. DOI: 10.1016/j.solener.2022.11.032.

[9] J. D. Gil et al. "A Review from Design to Control of Solar Systems for Supplying Heat in Industrial Process Applications". In: *Renewable and Sustainable Energy Reviews* 163 (July 1, 2022), p. 112461. ISSN: 1364-0321. DOI: 10.1016/j.rser.2022.112461.

[10] E. F. Camacho et al. "A Survey on Control Schemes for Distributed Solar Collector Fields. Part II: Advanced Control Approaches". In: *Solar Energy* 81.10 (Oct. 1, 2007), pp. 1252–1272. ISSN: 0038-092X. DOI: 10.1016/j.solener.2007.01.001.

[11] G. A. Andrade et al. "A Practical NMPC with Robustness of Stability Applied to Distributed Solar Power Plants". In: *Solar Energy* 92 (June 1, 2013), pp. 106–122. ISSN: 0038-092X. DOI: 10.1016/j.solener.2013.02.013.

[12] A. Nevado Reviriego, F. Hernández-del-Olmo, and L. Álvarez-Barcia. "Nonlinear Adaptive Control of Heat Transfer Fluid Temperature in a Parabolic Trough Solar Power Plant". In: *Energies* 10.8 (8 Aug. 2017), p. 1155. ISSN: 1996-1073. DOI: 10.3390/en10081155.

[13] S. Kamerling, V. Vuillerme, and S. Rodat. "MILP Algorithm for Outlet Temperature Optimization of a Hybrid Concentrated Solar System for SHIP Considering a 1D Solar Field and a Dual Phase Thermocline Storage". In: *Solar World Conference (SWC 2021)*. SWC2021 Proceedings. online, France: International Solar Energy Society, Oct. 2021. DOI: 10.18086/swc.2021.29.04.

[14] R. Dickes et al. "Dynamic Modeling and Control Strategy Analysis of a Micro-Scale CSP Plant Coupled with a Thermocline System for Power Generation". In: Conférence Eurosun 2014. Sept. 17, 2014. ISBN: 978-3-9814659-3-8.

[15] M. J. Vasallo and J. M. Bravo. "A MPC Approach for Optimal Generation Scheduling in CSP Plants". In: *Applied Energy* 165 (Mar. 1, 2016), pp. 357–370. ISSN: 0306-2619. DOI: 10.1016/j.apenergy.2015.12.092.

[16] J. Wang, Y. Li, and J. Zhang. "Coordinated Control of Concentrated Solar Power Systems with Indirect Molten Salt Storage Considering Operation Mode Switching: Using Switching Model Predictive Control". In: *Energy* 268 (Apr. 1, 2023), p. 126686. ISSN: 0360-5442. DOI: 10.1016/j.energy.2023.126686.

[17] N. Mohammadzadeh et al. "Model-Predictive Control for Dispatch Planning of Concentrating Solar Power Plants under Real-Time Spot Electricity Prices". In: *Solar Energy* 248 (Dec. 1, 2022), pp. 230–250. ISSN: 0038-092X. DOI: 10.1016/j.solener.2022.09.020.

[18] E. Girard et al. "Development and Evaluation of a Control Oriented Model to Optimize Industrial Heat Production of a Parabolic through Solar Power Plant". SolarPACES 2024 (Rome, Italy). Oct. 8, 2024.

[19] J. F. Hoffmann et al. "A Thermocline Thermal Energy Storage System with Filler Materials for Concentrated Solar Power Plants: Experimental Data and Numerical Model Sensitivity to Different Experimental Tank Scales". In: *Applied Thermal Engineering* 100 (May 5, 2016), pp. 753–761. ISSN: 1359-4311. DOI: 10.1016/j.applthermaleng.2016.01.110.

[20] T. Fasquelle et al. "A Thermal Model to Predict the Dynamic Performances of Parabolic Trough Lines". In: *Energy* 141 (Dec. 15, 2017), pp. 1187–1203. ISSN: 0360-5442. DOI: 10.1016/j.energy.2017.09.063.

[21] P. Ineichen and R. Perez. "A New Airmass Independent Formulation for the Linke Turbidity Coefficient". In: *Solar Energy* 73.3 (Sept. 1, 2002), pp. 151–157. ISSN: 0038-092X. DOI: 10.1016/S0038-092X(02)00045-2.

[22] Y. Karout et al. "Model-Based Predictive Control of a Solar Hybrid Thermochemical Reactor for High-Temperature Steam Gasification of Biomass". In: *Clean Technologies* 5.1 (1 Mar. 2023), pp. 329–351. ISSN: 2571-8797. DOI: 10.3390/cleantechnol5010018.